Spectroscopy and high-spin structure of ^{209}Fr

G. D. Dracoulis,[1,*] P. M. Davidson,[1] G. J. Lane,[1] A. P. Byrne,[2,1] T. Kibédi,[1] P. Nieminen,[1,†] H. Watanabe,[1,‡] and A. N. Wilson[1,2]

[1]*Department of Nuclear Physics, R. S. Phys. S. E., Australian National University, Canberra, A. C. T. Australia 0200*

[2]*Department of Physics, The Faculties, Australian National University, Canberra, A. C. T. Australia 0200*

(Received 5 March 2009; published 13 May 2009)

Excited states in ^{209}Fr have been studied using the ^{197}Au(^{16}O,4n)^{209}Fr reaction with pulsed beams and γ-ray and electron spectroscopy. A comprehensive scheme has been established up to an excitation energy of about 6 MeV and spins of about $49/2\hbar$. Several isomers have been identified including a $J^{\pi} = 25/2^{+}$, $\tau = 48(3)$ ns state at 2130 keV and a 606(26) ns, $45/2^{-}$ state at 4660 keV. The latter state decays via an enhanced $E3$ transition with a strength of 28.8(12) W.u. It can be identified with a similar isomer in the heavier odd isotopes ^{211}Fr and ^{213}Fr, arising from the maximal coupling of the five valence protons in the $\pi h_{9/2}^{3} i_{13/2}^{2}$ configuration. The systematics of the yrast states in the odd-A isotopes are discussed, including the presence of states arising from the main proton configurations coupled to the $p_{1/2}$, $f_{5/2}$, and $i_{13/2}$ neutron holes. Shell-model configurations are assigned to many of the observed states. The isotopic assignment differs from earlier work, which is shown to be erroneous.

DOI: 10.1103/PhysRevC.79.054313 PACS number(s): 21.10.Tg, 21.60.Cs, 23.20.Lv, 27.80.+w

I. INTRODUCTION

The identification of excited states in nuclei close to the $Z = 82$, $N = 126$ double shell closure has been an important part of the development of the understanding of the structure of heavy nuclei. With $Z = 87$, high-spin states in the francium isotopes are primarily formed by mutual alignment of the five valence protons distributed over the $h_{9/2}$, $f_{7/2}$, and $i_{13/2}$ orbitals directly above the proton Fermi surface. Such structures are known in some detail from the closed neutron shell at $N = 126$ and below [1,2], down to the $N = 124$ isotope ^{211}Fr [2]. In ^{213}Fr (and ^{212}Fr), neutron core excitations also become competitive at high spin, but this is less so in ^{211}Fr because of the depletion of the neutron core. For still lighter isotopes, the valence neutron holes are expected to play a more important role. In ^{210}Fr($N = 123$), a number of excited states have been assigned from the α decay of ^{214}Ac [3], but these are necessarily of relatively low spin, while a recent high-spin study by the Yale group reported a set of transitions for ^{210}Fr and a partial level scheme for ^{209}Fr [4]. However, our study does not agree with the latter assignments. As will be shown, these should be to the isotopes ^{209}Fr and ^{208}Fr, respectively, that is, moved down by one neutron number. This report is predominantly concerned with the structure of ^{209}Fr obtained from the new measurements, and the odd-A Fr isotopes. Complementary results and corresponding new assignments for ^{208}Fr are reported elsewhere [5]. Some information on the still lighter range of isotopes, $^{205-207}$Fr, has also recently been reported [6].

*Corresponding author: george.dracoulis@anu.edu.au

†Present address: Department of Physics, P. O. Box 35 (YFL) FIN-40014 University of Jyväskylä, Finland.

‡Present address: Nuclear Physics Research Division, RIKEN Nishina Center for Accelerator-based Science, 2-1 Hirosawa, Wako, Saitama, Japan 351-0198.

II. EXPERIMENTAL DESIGN AND ANALYSIS

The present results were obtained using mainly the (^{16}O, 4n) reaction on ^{197}Au. The measurements and analyses were carried out in conjunction with a study of the spectroscopy of ^{212}Rn as reported recently [7,8]. To address the discrepancy that has arisen between the present work and the earlier assignments [4] of transitions to ^{209}Fr and ^{210}Fr, our study also included measurements with ^{17}O and ^{18}O beams, the latter leading to the well-established case of ^{211}Fr, to provide an indirect calibration of the ^{16}O-induced reaction, as will be outlined below.

Pulsed beams of oxygen isotopes were provided by the 14UD Pelletron accelerator at the Heavy-Ion Accelerator Facility of the Australian National University. Pulses of about 1 ns in width and separated by 1716 ns were used in the main γ-γ–time measurements, which were complemented by γ-time measurements with a beam of nanosecond pulses separated by 19 μs.

The CAESAR array comprised six Compton-suppressed high-purity Ge detectors, three larger volume Ge detectors (also Compton suppressed and 80% efficient) and two LEPS detectors. The first six Compton-suppressed detectors in the array are arranged in the vertical plane, in pairs, at angles with respect to the beam direction of $\pm 97^{\circ}$, $\pm 148^{\circ}$, and $\pm 48^{\circ}$, allowing γ-ray anisotropies to be measured. The other detectors are in the horizontal plane.

γ-γ–time matrices were constructed from these data to establish the coincidence relationships. Where possible, additional time conditions were used to select γ rays feeding or following isomers. Lifetime information was obtained by projecting intermediate-time spectra from γ-γ–time cubes with gates on γ rays above and below the state of interest, as well as from several independent sets of γ-ray–time data obtained with the pulsed and chopped beams in the γ-ray and electron measurements (see below).

Angular anisotropy information was obtained from both the singles γ-ray measurements and the γ-γ coincidence data. The latter were obtained by constructing three matrices of

transitions observed in any of the three pairs of six detectors in the vertical plane (defining three angles with respect to the beam axis), on one axis, with either prompt or delayed transitions observed in the other eight large detectors. Gates were set to isolate specific transitions assigned to the scheme, without contamination. Spectra were constructed from which the three-point anisotropies could be determined. (These will be indicative of spin differences but are not sufficient to extract precise mixing ratios.) The angle and energy-dependent relative efficiencies required for the anisotropy determination were internally calibrated using the broad spectrum of lines produced in activity. The overall relative efficiency was determined using standard sources.

A number of conversion coefficients were measured directly using a superconducting solenoid to transport electrons to a cooled Si(Li) detector, with simultaneous measurement of γ rays in a single Compton-suppressed detector, in the arrangement described in Ref. [9]. The spectrometer was operated in the lens mode [9], allowing the selection of momentum ranges to optimize the efficiency for specific regions of the spectrum, as will be shown later. γ rays and electrons were measured with respect to a pulsed beam of ^{16}O ions, with pulses separated by 6.5 μs, conditions chosen to allow the subtraction of activities and other contaminants from the transitions associated with isomers in ^{209}Fr, by appropriate time-gating. This was imperative since it was found from the coincidence γ-ray results that nearly all of the main transitions assigned to ^{209}Fr were contaminated by activity lines. A target with a thickness of 2.4mg/cm^2 was placed with its plane at 30° to the beam axis. This thickness is a compromise between the need to simultaneously maintain electron resolution (with electrons observed through the back of the target and at 90° to the beam axis) and to stop most of the recoiling nuclei in the target.

III. RESULTS

A. Reaction conditions and isotopic assignments

Transitions in francium can be assigned unambiguously through coincidences with characteristic x rays. In the absence of mass selection, the assignment to a specific neutron number relies on an understanding of the xn cross sections and, in some cases, either prior information on low-lying transitions or complementary information from cross bombardments.

Although it becomes increasingly more difficult to populate neutron-deficient heavy nuclei because of fission competition, in the specific cases here, the cross sections are sufficiently large that special techniques are not necessary. Absolute cross sections for fusion evaporation reactions for ^{16}O incident on ^{197}Au are known to be in the region of 100–200 mb [10–12] with the dominant residues being the xn products, the francium isotopes. As fission competition becomes more important, the survival probability for cases where charged particles are evaporated is relatively increased, hence radon isotopes from the pxn evaporation channels are also observed.

The measurements were designed to populate high-spin states in ^{209}Fr through the ^{197}Au(^{16}O, 4n) reaction. On the basis of statistical model calculations, the peak of this reaction is expected at about 88 MeV. There have been several studies involving oxygen beams, which concur with this prediction (see, for example, Refs. [13,14]), and furthermore, the xn differential cross sections have been measured [10]. Although most of the cross-section studies involve measurement of the α activities for the known ground-state α decays, these are complicated by the fact that the α-particle energies for neighboring isotopes such as the pair ^{210,211}Fr and ^{208,209}Fr are not resolved within the pair (see, for example, Ref. [14]). However, the early study of Baba *et al.* [10] used the additional technique of mass separation to recover *individual* xn cross sections for ^{16}O on ^{197}Au. They report the peak of the 4n channel leading to ^{209}Fr to be at a center-of-mass energy of ∼82 MeV, corresponding to a beam energy of ∼89 MeV, in good agreement with our predictions and with their own calculations.

In the present work, a 5.5 mg/cm^2 target was used to ensure that most recoils would stop in the target, giving an average energy loss to the center of the target of about 4 MeV, hence the peak cross section should be covered at a beam energy of ∼92 MeV. This energy was chosen for ^{16}O in a comparison between ^{16}O, ^{17}O, and ^{18}O induced reactions on the same target. The beam energies for the ^{17}O and ^{18}O induced cases were adjusted to allow for the slightly less negative Q value for the 4n-evaporation channel in these cases. The energy integration because of the target thickness covers the main reaction yield directly above the Coulomb barrier, which is dominated by the 4n-evaporation channel. (On the basis of an excitation function with beam energies between 82 and 99 MeV, an ^{16}O beam energy of 95 MeV was subsequently chosen for the the main γ-γ–time measurements to improve the high-spin population with minimum contamination.)

The results of these singles measurements are shown in Fig. 1. The main transitions in the bottom panel (apart from the ^{197}Au Coulomb excitation) are the known transitions in ^{211}Fr, confirming that these reaction conditions will lead predominantly to the (^{18}O, 4n) channel. The main transitions marked in the top panel are those assigned in the present work to ^{209}Fr from the (^{16}O, 4n) reaction. This is in disagreement with Ref. [4], where the same transitions were assigned to ^{210}Fr.

Transitions in ^{210}Fr should, in fact, be evident in the middle panel, from the ^{17}O bombardment. The situation in this case is less clear than the other two because (a) the nuclide ^{210}Rn is populated through both the (expected) $p3n$ evaporation channel and also through the electron capture decay of the ground state of ^{210}Fr which is stronger and of higher spin than the equivalent decays in the odd-A isotopes, and (b) the energies of several of the main lines attributable to ^{210}Fr apparently overlap those of some of the ^{210}Rn lines. For example, the marked 817 keV γ ray is lower in energy than the 817.8 keV $2^+ \rightarrow 0^+$ transition in ^{210}Rn, which it partly overlaps [15]. Similarly, the 257 keV transition is both a line in ^{210}Rn from the decay of ^{210}Fr and a candidate transition in ^{210}Fr. The 203, 257, 520, 701, 721, and 817 keV lines were also observed in the γ-γ-coincidence studies of our earlier work with ^{12}C-induced reactions where the main population was to ^{211}Fr through the 5n channel with the contaminant 6n channel leading to ^{210}Fr [1].

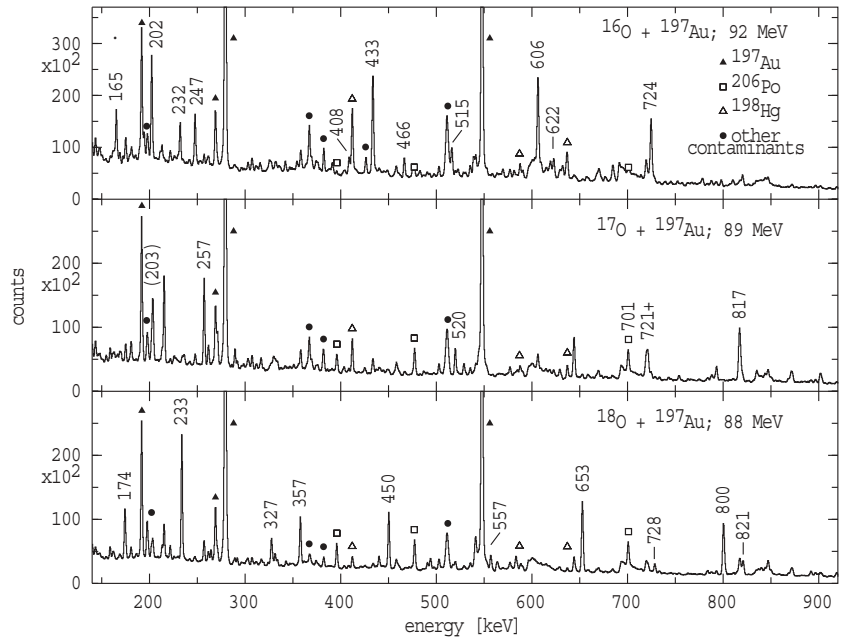

FIG. 1. Singles measurements with oxygen beams on ^{197}Au at energies appropriate for $4n$ evaporation. The energies of the main transitions assigned to francium isotopes are indicated.

Although the present γ-γ–time coincidence results confirm the arrangement of transitions and levels claimed in Ref. [4] with an isomeric state decaying through a 194 and 632 keV cascade, from our excitation function results and cross bombardments, we assign it to ^{208}Fr, rather than to ^{209}Fr. (A report on ^{208}Fr has been published [5], and ^{210}Fr will be the subject of a later study.) We note also that although the Yale group reported a cross bombardment with the ^{37}Cl-induced reaction on ^{176}Yb, their beam energies seem to be well in excess of the energies appropriate for the population of ^{210}Fr and ^{209}Fr, consistent with significant production of ^{208}Fr. They also show excitation functions (Fig. 2, Ref. [4]) but as noted earlier, fission competition which becomes more prevalent at higher energies has the effect of favoring channels that involve proton emission. The competition can result in a difference in energy dependence (and therefore peak energies) for $5n$ evaporation compared to $1p4n$ evaporation, for example, and compromise interpretations based on the shape of excitation functions.

Finally, the main activity lines (as observed in the long time region with the 19 μs pulsing) can be attributed to the $A = 209$ and $A = 208$ decay chains (both electron capture and α-decay paths), with an insignificant amount attributable to $A = 210$. This is consistent with the recent use of the (^{16}O, $4n$) reaction at 91 MeV to populate ^{209}Rn via activity [16].

B. ^{209}Fr level scheme

Transitions assigned to ^{209}Fr are listed in Table I together with their placement in the scheme, relative intensities, and, where available, anisotropies. The anisotropies are given in terms of the normalized coefficient in a fit to an expansion, up to second order, in the Legendre polynomial.

The level scheme is shown in Fig. 2. γ-γ coincidence spectra that illustrate some key features of the scheme are given in Fig. 3. The 539 keV coincidence gate (with a $\pm$150 ns time-difference condition) selects out transitions in the path parallel to the main cascade between the 1764 keV state and the ground state. The 433 and 724 keV transitions that carry the main cascade intensity are not evident in this spectrum, which shows the two alternative paths via the 136, 466, and 622 keV transitions to ground, and the 619 and 606 keV transitions from the decay of the 1225 keV state. The complication is that there are three close-lying transitions in the scheme, with energies of 618.9 and 622.7 keV from this path, and the 620.2 keV transition placed in the upper part of the scheme, as a direct decay from the longer-lived isomer.

The feeding from two strongly populated isomers is evident in the coincidence gates for the 202 keV transition in the short-delayed time region (35–175 ns) compared to the more delayed region (175–1500 ns), with the shorter isomer being lower in the scheme and more strongly populated. In comparison, the gate on the 232 keV line shows the main lines from the upper isomer (620, 409, 516, and 691 keV) with an intensity essentially equal to that of the lowest cascade through the 433 and 724 keV transitions. There is also a weakly populated isomeric state feeding the 3234 keV state (Fig. 2) through a 181 keV transition with a lifetime intermediate between that assigned to the 2130 keV state and to the 4660 keV state (see Fig. 2).

Also marked in these spectra is a 45 keV transition, which is more clearly seen in the coincidence spectrum obtained with the LEPS detector shown in Fig. 4. This transition is placed as the connection between the 2175.8 and 2130.4 keV states, the latter of which has a lifetime.

Also, in the level scheme, the 248.8 keV transition is placed in parallel to the strong 231.7 keV transition and in the main decay path, implying an unobserved 17.1 keV transition between the 2424.6 and 2407.5 keV states. This energy gap is independently confirmed by the two decay paths from the 3234.4 keV state via the 809.8 keV transition to the 2424.6 keV state and via the 331.2/727.4 keV cascade to the 2175.8 keV state.

TABLE I. Properties of transitions assigned to ^{209}Fr.

E_γ [a]	I_γ [a]	A_2/A_0 [b]	E_i	E_f	J_i^π	J_f^π
17.1	*509(98)*		2424.6	2407.5	$29/2^+$	$27/2^+$
45.4	18(3)		2175.8	2130.4	$25/2^+$	$25/2^+$
136.1	42(6)	−0.31(7)	1225.0	1088.9	$17/2^-$	$15/2^-$
(140.3)			(2857.6)	2717.3		(29/2)
164.9	261(11)	−0.24(4)	1928.5	1763.6	$23/2^-$	$21/2^-$
174.9	26(2)	−0.45(12)	3409.3	3234.4	$33/2^{(+)}$	$31/2^{(+)}$
181.4	13(2)	(−0.19(20))	3415.8	3234.4	$33/2^{(-)}$	$31/2^{(+)}$
201.9	510(10)	−0.12(5)	2130.4	1928.5	$25/2^+$	$23/2^-$
231.7	261(8)	−0.58(4)	2407.5	2175.8	$27/2^+$	$25/2^+$
247.3	350(10)	−0.24(4)	2175.8	1928.5	$25/2^+$	$23/2^-$
248.8	42(8)	+0.18(11)	2424.6	2175.8	$29/2^+$	$25/2^+$
284.7	26(2)	−0.32(13)	4324.2	4039.5	$41/2^+$	$39/2^+$
309.8			2717.3	2407.5	(29/2)	$27/2^+$
331.2	41(3)	−0.40(13)	3234.4	2903.2	$31/2^{(+)}$	$29/2^+$
335.5	10(2)	+0.09(27)	4659.7	4324.2	$45/2^-$	$41/2^+$
342.2	15(2)	−0.45(20)	3369.5	3027.3	$33/2^+$	$31/2^+$
(386.4)	3(1)			4659.7		$45/2^-$
408.7	131(6)	−0.46(7)	4039.5	3630.8	$39/2^+$	$37/2^+$
414.9	9(2)	−0.50(16)	5903.3	5488.4	$49/2^-$	$47/2^-$
433.2	937(14)	+0.26(5)	1763.6	1330.4	$21/2^-$	$17/2^-$
435.7			3153.0	2717.3	$31/2^-$	(29/2)
466.3	182(5)	+0.21(5)	1088.9	622.7	$15/2^-$	$11/2^-$
481.4	46(4)	−0.34(17)	2245.0	1763.6	$23/2^+$	$21/2^-$
482.7	67(4)	−0.48(17)	1088.9	606.0	$15/2^-$	$13/2^-$
514.0	48(9)	−0.53(24)	3923.3	3409.3	$35/2^{(+)}$	$33/2^{(+)}$
515.5	231(9)	+0.38(10)	3630.8	3115.3	$37/2^+$	$33/2^+$
528.3	61(5)	+0.44(16)	3127.3	2599.0	$31/2^-$	$27/2^-$
534.8	6(1)	−0.45(11)	5194.5	4659.7	$47/2^{(-)}$	$45/2^-$
538.7	250(10)	+0.20(9)	1763.6	1225.0	$21/2^-$	$17/2^-$
559.3	60(8)	−0.19(4)	3968.6	3409.3	35/2	$33/2^{(+)}$
566.2	45(5)	−0.65(14)	2696.2	2130.4	$27/2^+$	$25/2^+$
602.7	85(4)	−0.57(8)	3027.3	2424.6	$31/2^+$	$29/2^+$
606.0	1000(16)	+0.27(3)	606.0	0.0	$13/2^-$	$9/2^-$
618.9	159(20)	+0.23(9)	1225.0	606.0	$17/2^-$	$13/2^-$
620.2	75(5)	+0.07(12)	4659.7	4039.5	$45/2^-$	$39/2^+$
622.7	228(8)	−0.43(10)	622.7	0.0	$11/2^-$	$9/2^-$
630.5	33(3)	−0.60(12)	2559.0	1928.5	$25/2^{(-)}$	$23/2^-$
642.3	5(1)	−0.23(19)	5302.0	4659.7	47/2	$45/2^-$
670.5	52(4)	+0.33(9)	2599.0	1928.5	$27/2^-$	$23/2^-$
690.7	275(11)	+0.25(5)	3115.3	2424.6	$33/2^+$	$29/2^+$
692.7	13(2)		2937.7	2245.0	(27/2)	$23/2^+$
724.4	989(17)	+0.23(4)	1330.4	606.0	$17/2^-$	$13/2^-$
727.4	60(10)	(+0.26(9))	2903.2	2175.8	$29/2^+$	$25/2^+$
728.4	30(10)		3153.0	2424.6	31/2	$29/2^+$
733.2	21(3)	−0.63(17)	4364.0	3630.8	$39/2^+$	$37/2^+$
739.7	17(2)	+0.39(8)	5399.4	4659.7	$49/2^-$	$45/2^-$
745.0	15(3)		5069.2	4324.2	(43/2)	$41/2^+$
745.5	22(2)	(+0.22(11))	3153.0	2407.5	31/2	$27/2^+$
(754.1)	2(1)			4659.7		$45/2^-$
757.0	15(2)		4166.3	3409.3	(37/2)	$33/2^{(+)}$
787.4	60(3)	+0.30(11)	2917.8	2130.4	$29/2^{(+)}$	$25/2^+$
792.7	34(3)	+0.33(14)	4423.5	3630.8	$41/2^{(+)}$	$37/2^+$
809.8	93(8)	−0.10(8)	3234.4	2424.6	$31/2^{(+)}$	$29/2^+$
(820.5)	2(1)			4659.7		$45/2^-$

TABLE I. *(Continued.)*

E_γ[a]	I_γ[a]	A_2/A_0[b]	E_i	E_f	J_i^π	J_f^π
828.7	17(2)	−0.66(6)	5488.4	4659.7	$47/2^-$	$45/2^-$
997.4	5(1)	−0.56(13)	5657.1	4659.7	$47/2^-$	$45/2^-$
1105.4	4(1)	−0.32(13)	5765.1	4659.7	47/2	$45/2^-$

[a]Unobserved transitions have implied energy and total transition intensities in italics. The uncertainty in energies range from ±0.15 keV for strong lines to ±0.25 keV for weak lines.
[b]From a three-point anisotropy.

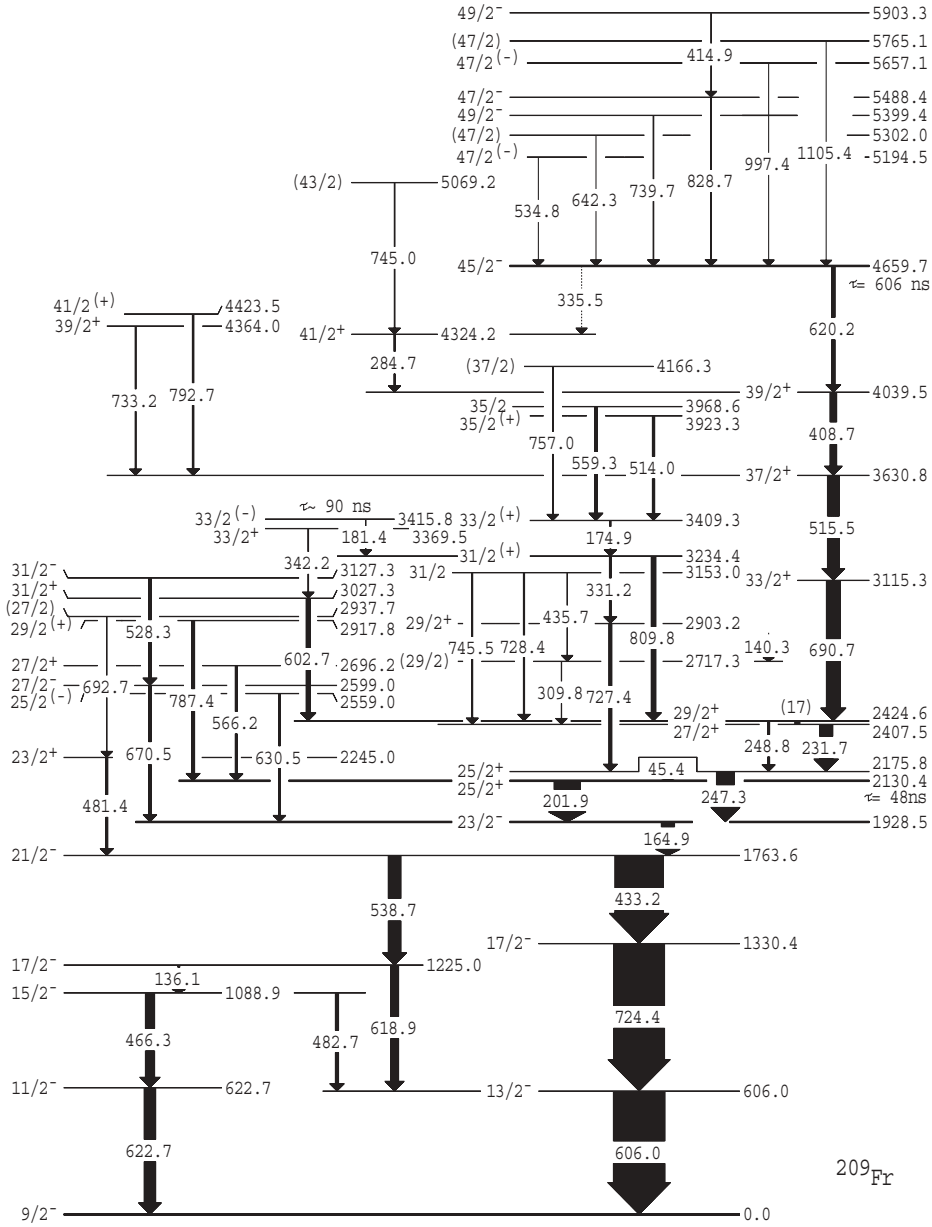

FIG. 2. Level scheme of ^{209}Fr from the present study.

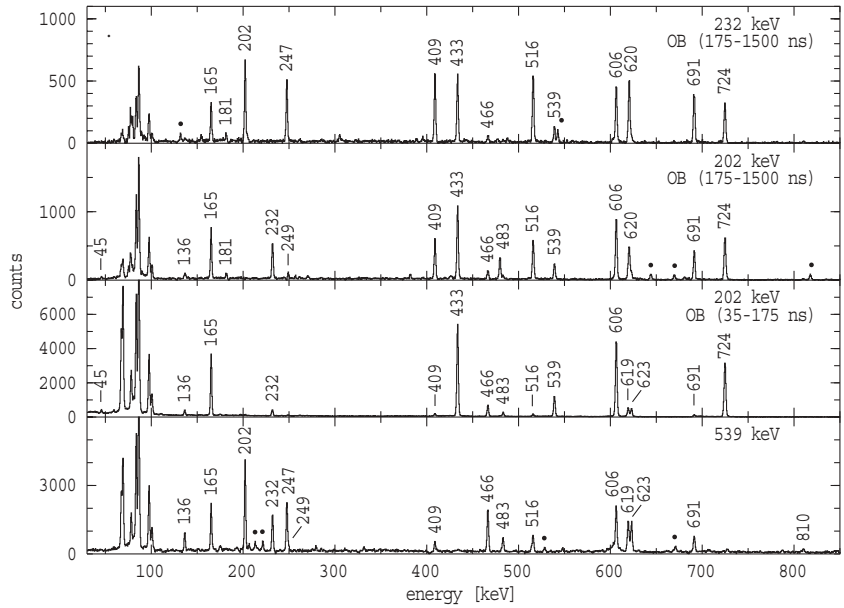

FIG. 3. γ-γ-coincidence spectra with gates on individual transitions. The upper three panels have additional time gates selecting the out-of-beam region as indicated. (Target x rays from random coincidences are observed, as well as the characteristic francium x rays.)

The 248.8 keV transition is in coincidence with all transitions in the main (delayed) cascade, and although the line is only partially resolved in the large detectors from the much more intense 247.3 keV line, with which it is in coincidence, it is more clearly resolved in the LEPS detectors. This is illustrated in Fig. 5. Note the low intensity of the 248.8 keV line compared to both the 247 and 232 keV lines.

Transitions that feed the uppermost isomer are seen in the "early" spectrum with gates on the several lines in cascade below the isomer, shown in Fig. 6. (Only the strongest of these early lines have been placed in the level scheme.) The main transitions that follow the isomer are evident in the "delayed" spectrum constructed with gates on the two strongest lines above the isomer. The line marked as a contaminant at 181 keV is associated with a 740 keV γ ray, arising probably from ^{99}Tc, one of the fission products.

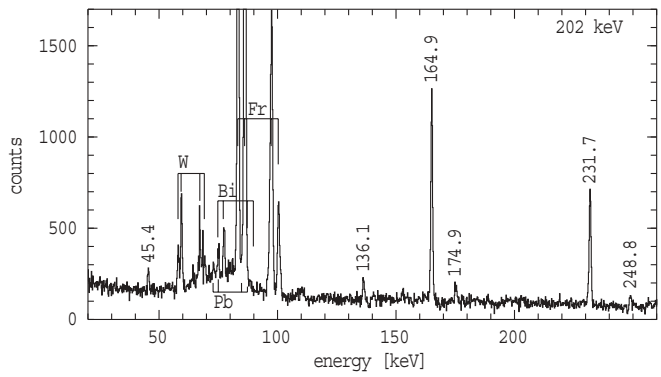

FIG. 4. γ-γ-coincidence spectrum as observed in the LEPS detector with a gate on the 202 keV transition and a $\pm$150 ns time-difference condition. (As well as the characteristic x rays from francium, x rays from tungsten, bismuth, and lead are also observed due to fluorescence in the shielding material near the LEPS detectors.)

With respect to the level scheme shown in Fig. 2, except for several transitions that appear in the early spectrum that have not been placed in the scheme as noted above, which could be additional parallel feeds directly to the isomer, essentially all transitions that can be firmly assigned to ^{209}Fr have been placed. There are some residual uncertainties, such as the ordering of the 331.2/727.4 keV cascade from the 3234.4 keV state: the alternative ordering would place an intermediate state at 2507.0 rather than at 2903.2 keV. Also, there are several complications associated with γ rays at 181 keV (noted earlier) and at 140 and 175 keV which arise from fission products and their complementary partners but which have close-lying γ rays in ^{209}Fr.

C. Conversion coefficients

As well as the direct measurement of conversion coefficients to be discussed below, there are a number of cases for which it has been possible to extract total internal conversion

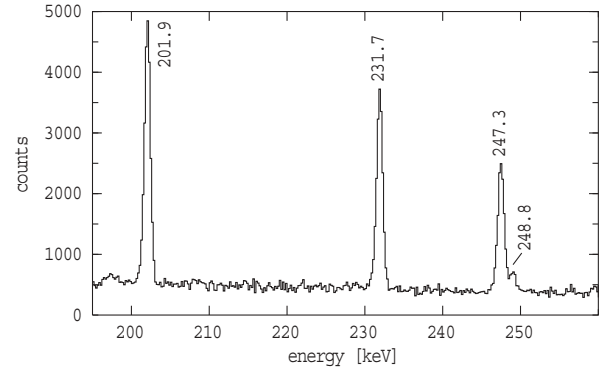

FIG. 5. γ-γ-coincidence spectrum as observed in the LEPS detector produced by summing gates on the main cascade lines in the delayed time region.

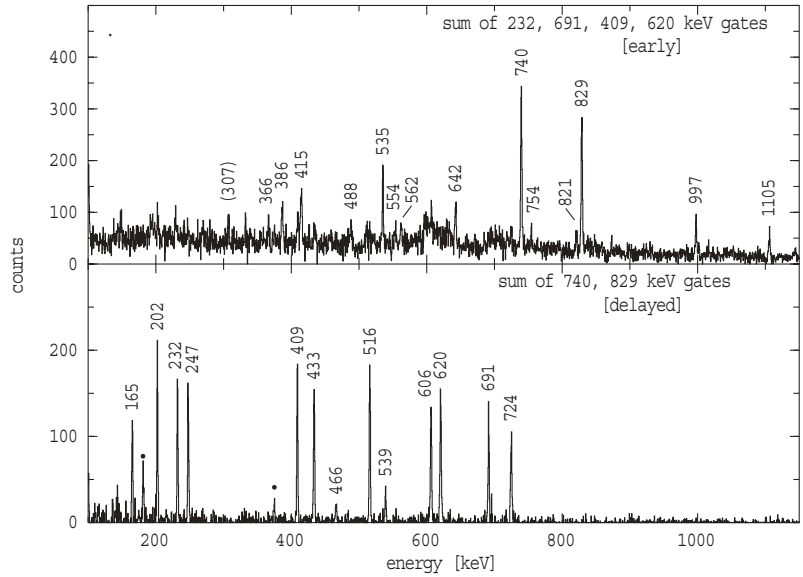

FIG. 6. Time-correlated γ-ray coincidence spectra with time difference gates of -150 to -1500 ns ("early") or $+150$ to $+1500$ ns ("delayed") and γ-ray gates as indicated.)

coefficients for individual lines or combinations of lines from intensity balances, and thus restrict multipolarities and spin assignments, particularly for low-energy transitions. In the 539 keV γ-γ coincidence spectrum shown in Fig. 3, for example, the 136 keV γ-ray total intensity has to balance the sum of the 466 and 483 keV decay paths, while the 466 keV intensity has to balance that of the 622 keV transition. Similar analyses resulted in the total conversion coefficients for the 45, 136, 165, 175, 181, 202, 232, 247, and 409 keV lines listed in Table II.

Several K and L conversion coefficients for specific transitions are listed in Table II together with the theoretical values for selected multipolarities. Some were obtained with

TABLE II. Conversion coefficients in ^{209}Fr.

E_γ	Type	Experiment	Assignment[a]	Theory[b]			
				$E1$	$M1$	$E2$	$E3$
45.4	T	28.0(8)	$M1$	0.883	28.3	385	2.2×10^4
136.1	T	7.0(10)	$M1$	0.224	5.96	2.43	43.0
164.9	T	3.08(11)	$M1$	0.140	3.46	1.13	15.5
174.9	T	1.8(3)	$M1+E2$	0.122	2.93	0.906	11.4
181.4	T	0.24(15)	$E1$	0.112	2.64	0.790	9.46
201.9[c]	T	$\leqslant$0.091(53)	$E1$	0.086	1.95	0.534	5.52
231.7	T	1.33(13)	$M1$	0.062	1.33	0.331	2.83
247.3[a]	T	$\leqslant$0.091(53)	$E1$	0.053	1.11	0.266	2.08
408.7	T	0.25(13)	$M1+E2$	0.017	0.28	0.061	0.26
	K	0.145(14)		0.014	0.23	0.037	0.094
	L	0.012(4)		0.0025	0.041	0.018	0.122
433.2	K	0.032(2)	$E2$	0.0125	0.194	0.033	0.083
	M	0.003(1)		0.0005	0.008	0.0038	0.026
466.3	K	0.031(3)	$E2$	0.0107	0.159	0.028	0.071
482.7	K	$\geqslant$0.065(11)	$M1+E2$	0.010	0.145	0.026	0.066
538.7	K	0.019(3)	$E2$	0.008	0.108	0.021	0.052
606.0	K	0.016(2)	$E2$	0.0064	0.079	0.017	0.041
	L	0.007(1)		0.0011	0.014	0.005	0.024
618.9	K	0.017(3)	$E2$	0.006	0.075	0.016	0.039
622.7	K	0.057(4)	$M1+E2$	0.006	0.074	0.016	0.038
620.0	K	0.042(8)	$E3$	0.0061	0.075	0.016	0.039
	K/L	1.6(3)		6.01	5.62	3.29	1.73
724.4	K	0.012(2)	$E2$	0.005	0.050	0.012	0.028
	L	(0.0022(4))		0.001	0.009	0.003	0.013

[a]Main component. Also, see anisotropy and lifetime analyses.
[b]Reference [17].
[c]Combined analysis.

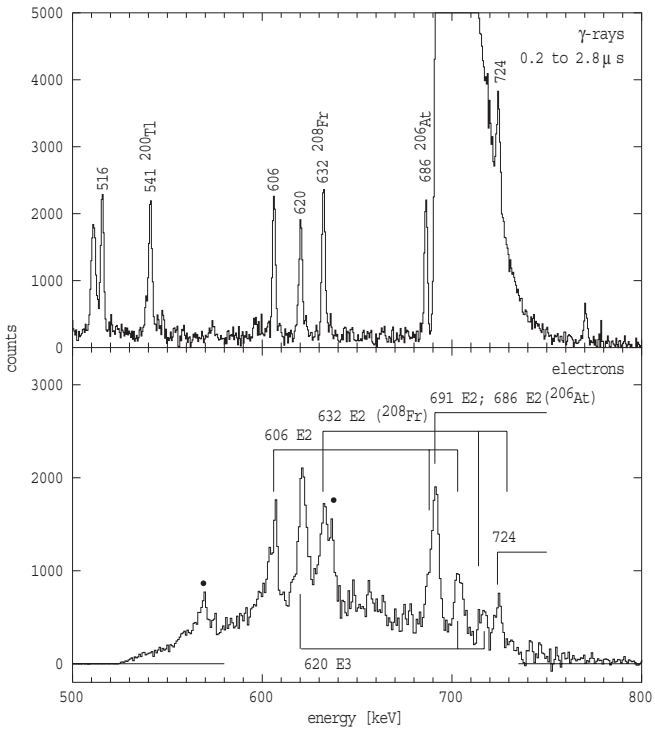

FIG. 7. γ-ray and electron spectra obtained in a configuration with the electron momentum range centered on transitions near the 620 keV direct decay from the 606 ns high-spin isomer. The electron spectrum has been shifted up in energy so that the lines from K conversion in francium align with the γ-ray transition energies. The bars in the lower panel indicate the position of K, L, and M lines from each transition. (Contaminants are indicated by filled circles.)

time gates to select transitions that were either prompt or populated by the relatively short-lived isomer ($\tau = 48$ ns) at 2130 keV through which most of the decay proceeds, and a broad momentum selection range for the electrons, scanning in the region between about 100 and 900 keV. However, because of the low population of the high-spin isomer at 4660 keV (about 5% relative to the lower spin cascade), it was necessary to constrain the momentum range to obtain sufficient intensity for the main decay. Figure 7 shows corresponding γ-ray and electron spectra with the electron momentum range focused on a narrow region to take in the 620 keV transition that is the direct decay from the isomer, bracketed by the 606 and 632 keV transitions from the low-spin yrast cascades in ^{209}Fr and ^{208}Fr, respectively. Both γ-ray and electron spectra are constructed with equivalent time gates, selecting the 0.3–3.0 μs region after the beam pulse, with the subsequent time region of 3.0–5.7 μs subtracted, in order to capture the main intensity of the isomer and remove long-lived contaminants. As well as the broad Ge (n, n') line in the γ-ray spectrum, which masks the 691 keV transition in the high-spin cascade, the 632 keV transition in ^{208}Fr is also observed as is the 686 keV transition in ^{206}At [5,18], both of which arise from isomers with a similar lifetime. Note also that with a narrow momentum selection (giving a higher electron efficiency compared with the broad range mode), the electron efficiency is not constant [9].

Both the 606 and 632 keV lines are established as having $E2$ multipolarity (in the present work). Comparing the electron and γ-ray spectra, it is apparent that the 620 keV line has a larger K-conversion coefficient. Although the 620 keV γ-ray line is mainly due to the 620.2 keV transition from the isomer, it also contains two other (weak) components that are partially resolved in the γ-ray detector, the 618.9 keV $(17/2^- \rightarrow 13/2^-)$ $E2$ transition (see Fig. 2) and the 622.7 keV $(11/2^- \rightarrow 9/2^-)$ $M1$ transition, both of which have multipolarities established independently in this work. These components are taken into account in extracting the K- and L-conversion coefficients given for the 620.2 keV transition in Table II. Note also that the electron line observed at an electron energy equivalent to the 691 keV γ-ray transition in ^{209}Fr is a combination of that line and the electron line from K conversion of the 686 keV ($E2$) transition in ^{206}At [5,18].

D. Lifetimes and transition strengths

Lifetimes were established from a number of sources including timing with respect to the pulsed beam and also from the time-γ-γ data. Examples of the time spectra obtained with the 1 ns / 19 μs pulsing conditions are shown in Fig. 8. The top panel is a sum of gates on uncontaminated transitions in the main cascade from the uppermost isomer observed, with a fit including the prompt component to each of the states in the path included. The lifetime obtained is 606(20) ns. The

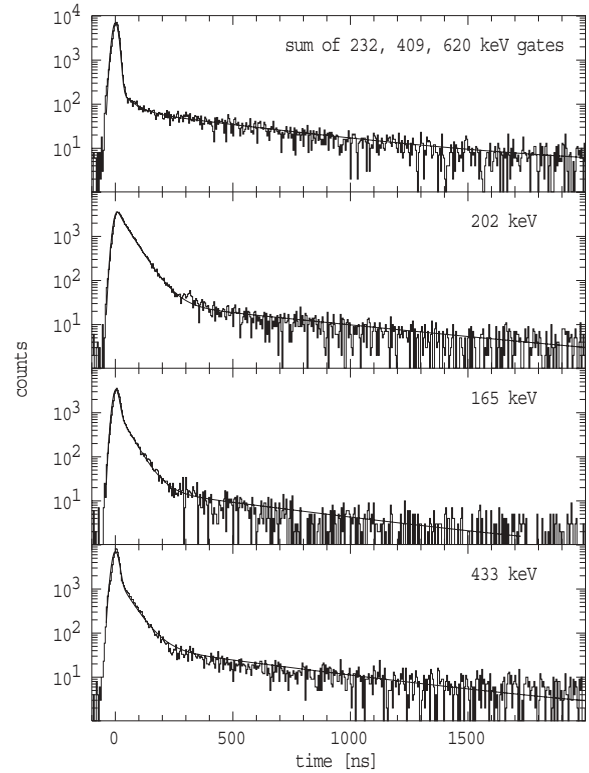

FIG. 8. Time spectra obtained with the 1 ns/19 μs pulsing with gates on selected transitions as indicated. The full curves are fits including the measured prompt response function and the feeding through prompt and isomeric paths.

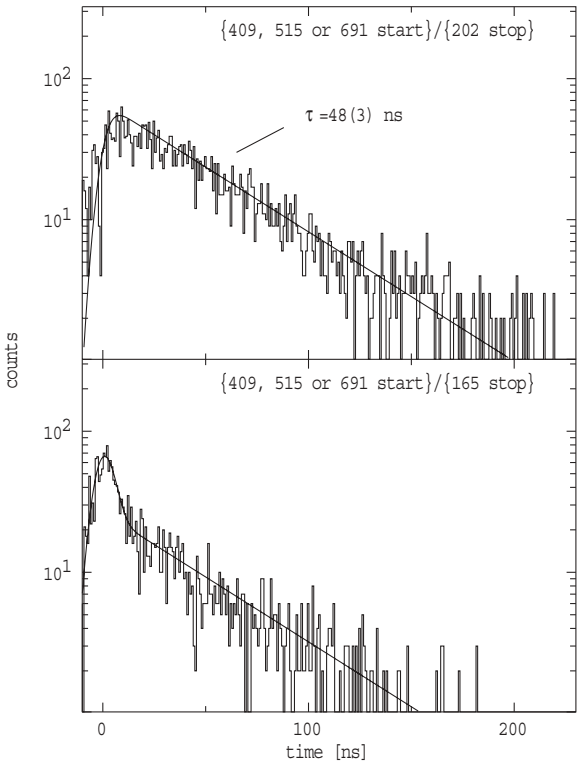

FIG. 9. Intermediate time spectra obtained with "start" gates in the large Ge detectors, and "stop" gates on γ rays measured in the LEPS detector.

time curve for the 202 keV transition shows a 48 ns lifetime as well as feeding from the longer-lived isomer above, whereas the 165 keV transition placed below the 202 keV transition in the level scheme shows both prompt feeding and feeding from both isomers above. The prompt component is principally from the path via the 247 keV transition depopulating the state at 2176 keV, which does not have a significant lifetime. Similarly, the time curve for the 433 keV transition has a complex shape, consistent (in detail) with the proposed level scheme. Although not shown here, the 181 keV transition that feeds the 3234 keV state shows a lifetime of about 90 ns. As shown in the level scheme (Fig. 2), we have not identified any transitions feeding this state to be able to confirm the lifetime through the time–γ-γ data, although consistent delayed components are observed in the time spectra for transitions that follow, such as the 810 keV line.

The lifetime of the 2130 keV state can be isolated, however, in the time–γ-γ data with gates on the transitions that feed (passing through states that have no significant lifetime) and the 202 keV transition that depopulates that state. An example is shown in Fig. 9 extracted from the coincidence data where the 202 keV transition is observed in the LEPS detector, which has a superior time response for low-energy transitions. The absence of a prompt component in this spectrum, consistent with its placement as a direct decay from an isomer, is in contrast to the equivalent spectrum constructed with a gate on the 165 keV transition. As mentioned above, it is fed via both a prompt path (through the 247 keV transition) and the 202 keV decay from the isomer.

Transitions strengths for selected states in ^{209}Fr, including values deduced from lifetime limits in the cases of strongly populated states with low-energy decays in the main cascade, are given in Table III.

E. Spin and parity assignments

Assignments have been made taking into account all the available experimental information including anisotropies, transition strengths, and conversion coefficients. Some key points can be made that lead to a number of firm assignments. At low spins, the 606, 724, and 433 lines that carry the main intensity can be characterized as stretched $E2$ transitions, giving spins and parities of $13/2^-$, $17/2^-$, and $21/2^-$ for the 606, 1330, and 1764 keV states, respectively. In the parallel path, the 622.7 keV transition to ground and the 466 keV line that feeds it are dipole and quadrupole transitions, respectively. No significant lifetimes are observed here, so $M2$ multipolarity can be eliminated for the 466 keV line, whose K conversion also defines it as an $E2$ transition. The total conversion coefficient for the 136 keV line (Table II) defines it as $M1$; and this, together with the decay from the 1764 keV $21/2^-$ state via the 539 keV $E2$ transition to the 1225 keV state and branches from both the 1225 and 1089 keV states to the 606 keV $13/2^-$ state, leads to the assignments of $17/2^-$, $15/2^-$, and $11/2^-$ for the 1225, 1089, and 623 keV states, respectively. The 433 and 539 keV transitions are then competing $E2$ decays from the same state. The strong favoring of the lower energy transition, despite the E_γ^5 energy factor, is attributed later to the difference in configuration between the initial and final states.

The 165 keV transition is a dipole with a conversion coefficient that is close to the $M1$ value (with a small $E2$ component), thus eliminating an $E1$ possibility, leading to $J^\pi = 23/2^-$ for the 1929 keV state. The situation with the pair of states at 2130 and 2176 keV is complicated, but the analysis leads to a clear assignment for both. On the basis of intensity balances from a number of sources, the total conversion coefficients for each transition must be small. This leads to a definitive $E1$ assignment for the 202 keV transition and a probable $E1$ assignment for the parallel 247 keV transition as well, although $E2$ cannot be completely eliminated for the latter transition on this basis alone, because of its slightly higher energy. However, the angular distributions say that both are dipoles and therefore $E1$ (and, because of the low conversion, not $M1$). Independently, since the 45.4 keV transition to the $25/2^+$, 2130 keV state can be characterized as an $M1$ (Table II), the 2175 keV state can only have either $J^\pi = 25/2^+$ or $27/2^+$. However, the higher spin can be eliminated, since it would require the 247 keV transition to be an $M2$, which would imply both a very large conversion coefficient for the transition and a long lifetime for the 2176 keV state, neither of which is observed. The 2176 keV state lifetime is in fact short, within the present limit of sensitivity of about a nanosecond for strong lines, while the 2130 keV state has a 48 ns lifetime.

The total conversion coefficient for the 232 keV transition defines it as an $M1$, and this together with its negative anisotropy leads to the $27/2^+$ assignment for the 2408 keV

TABLE III. Branching ratios and transition strengths for selected states in ^{209}Fr.

Initial state τ	Final state J^π	E_γ (keV)	I_γ [a]	$\sigma\lambda$	α_T	$B(\sigma\lambda)$ (e^2 fm$^{2\lambda}$ or μ_0^2 fm$^{(2\lambda-2)}$)	Transition strength (W.u.)
$45/2^-$ 4660 keV							
606(26) ns	$39/2^+$	620.2	100.0(2)	$E3$	0.0686	$7.48(32) \times 10^4$	28.8(12)
	$41/2^+$	335.5	1.1(2)	$M2$	1.602	$2.85(32) \times 10^{-1}$	$4.9(9) \times 10^{-3}$
$29/2^+$ 2425 keV							
<1.0 ns	$25/2^+$	248.8	42(8)	$E2$	0.261	>63.6(14)	>0.86(19)
	$27/2^+$	17.1	*4.1(3)* [b]	$M1$	124	$>8.1(11) \times 10^{-2}$	$>4.5(6) \times 10^{-2}$
$25/2^+$ 2176 keV							
<1.0 ns	$23/2^-$	247.3	350(10)	$E1$	0.0533	$>1.62(23) \times 10^{-5}$	$>7.1(1) \times 10^{-6}$
	$25/2^+$	45.4	18(3)	$M1$	28.3	$>1.22(27) \times 10^{-2}$	$>6.8(15) \times 10^{-3}$
$25/2^+$ 2130 keV							
48(3) ns	$23/2^-$	201.9	100	$E1$	0.0862	$1.46(9) \times 10^{-6}$	$6.4(4) \times 10^{-7}$
$23/2^-$ 1929 keV							
<1.5 ns	$21/2^-$	164.9	100	$M1$	3.46	$>1.90(13) \times 10^{-3}$	$>1.06(7) \times 10^{-3}$

[a]Relative intensities.

[b]γ-ray intensity deduced from total intensity balances and assuming pure $M1$ multipolarity.

state. The 2425 keV state directly above is connected by the unobserved 17 keV transition, and although the conversion coefficient of the 249 keV transition cannot be easily extracted because of the proximity of the much stronger 247 keV transition, its anisotropy suggests a quadrupole (and therefore $E2$ rather than $M2$ multipolarity in the absence of a lifetime) leading to $J^\pi = 29/2^+$ for the 2425 keV state. It is also the case that the 2130 keV state is fed by only a few transitions that bypass the 2425 keV state, consistent with the 2425 keV state being of higher spin, although by itself, this is not a strong argument.

Considering the main transitions that proceed in cascade from the higher-lying isomer, only the 409 keV transition is sufficiently low in energy that a total conversion coefficient can be extracted from intensity balances (see Table II), and it suggests $M1$ multipolarity. The anisotropies for the 691 and 516 keV γ rays are consistent with stretched quadrupoles, while the absence of significant lifetimes for the initial states eliminates $M2$, consistent with the absence of high internal conversion. This, and the (mixed) dipole character of the 409 keV transition, leads to the $33/2^+$, $37/2^+$, and $39/2^+$ assignments to the 3115, 3631, and 4040 keV states, respectively. While a significant angular distribution cannot be extracted for the 620 keV transition from the isomer, both because it overlaps with a number of close-lying transitions and because of attenuation due to the relatively long lifetime, its conversion coefficients suggest $E3$ multipolarity, leading to a natural explanation for the presence of an isomer, as will be discussed in the section on configuration assignments. The 4324 keV state that decays via a 285 keV transition to the $39/2^+$ state is relatively strongly populated and is tentatively assigned as $41/2^+$. It is observed weakly in coincidence with the lower cascade in the out-of-beam time region, consistent with the presence of a weak branch (335.5 keV) to it from the $45/2^-$ isomer.

For the states not in the main cascade, while many of the transitions are relatively weak, the measured anisotropies provide significant constraints on the spins and parities. For example, the 671 keV transition to the $23/2^-$ 1929 keV state has a positive anisotropy and (given the absence of a significant lifetime) is probably a stretched $E2$, a possible $J \rightarrow J$ alternative being unlikely given the population of the 2599 keV state. That gives $J^\pi = 27/2^-$ for that state. It is fed by the 528 keV transition which also has a positive anisotropy, hence a suggested assignment of $31/2^-$ for the 3127 keV state. In contrast, the 566 and 631 keV transitions that feed the $25/2^+$ and $23/2^-$ states both have large negative anisotropies, suggesting mixed $M1/E2$ transitions, and therefore $J^\pi = 27/2^+$ and $25/2^-$ for the 2696 and 2559 keV states, respectively. A similar argument applies to the 603 keV transition leading to an assignment of $31/2^+$ for the 3027 keV state.

The 810 keV branch from the 3234 keV state to the 2425 keV $29/2^+$ state is a dipole but with a relatively small anisotropy, hence the 3234 keV state could be either positive or negative parity. The other main branch is via the 331.2, 727.4 keV cascade, transitions which are probably mixed-dipole and quadrupole (presumably $E2$), respectively, giving a $29/2^+$ assignment for the 2903.2 keV intermediate state and favoring positive parity for the 3234 keV state, hence the suggested assignment of $J^\pi = 31/2^{(+)}$. From its angular distribution and total conversion coefficient (Table II), the 174.9 keV transition is mixed $M1/E2$, leading to $33/2^{(+)}$ for the 3409 keV state.

Similar considerations lead to the other suggested assignments, but these will not be discussed in detail here.

IV. DISCUSSION

A. Configurations

In moving away from the closed neutron shell at $N = 126$, the possible shell-model configurations that will produce relatively low-lying states increases quickly. The configurations that will give rise to multiplets involve the main proton excitations (as calculated for ^{213}Fr in Ref. [1]) coupled to

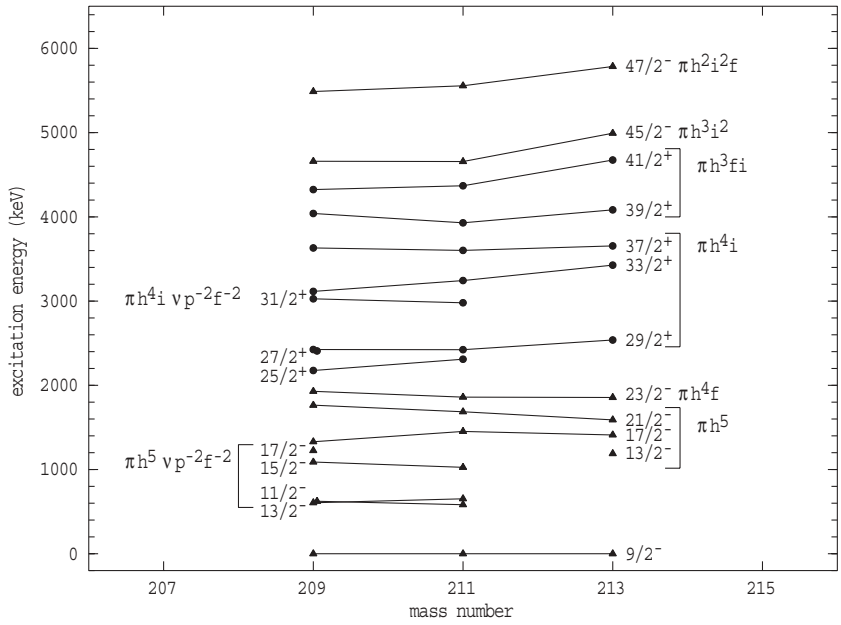

FIG. 10. Systematic of selected states in the odd-A francium isotopes.

several neutron-hole combinations. The proton components listed in hierarchical order with their maximum spins include

$$\begin{aligned}
&\pi h_{9/2}^5; && J_{\max} = 25/2^-,\\
&\pi h_{9/2}^4 f_{7/2}; && J_{\max} = 31/2^-,\\
&\pi h_{9/2}^4 i_{13/2}; && J_{\max} = 37/2^+,\\
&\pi h_{9/2}^3 f_{7/2} i_{13/2}; && J_{\max} = 41/2^+,\\
&\pi h_{9/2}^3 i_{13/2}^2; && J_{\max} = 45/2^-,\\
&\pi h_{9/2}^2 i_{13/2}^3; && J_{\max} = 49/2^+.
\end{aligned}$$

The corresponding neutron excitations are exemplified by the spectrum of ^{204}Pb [19] with the four neutron holes coupled to spin zero being the ground state and levels from the configurations (listing only the main couplings)

$$\begin{aligned}
&\nu\left[p_{1/2}^{-2}\right]_{0^+}, f_{5/2}^{-2}; && J_{\max} = 4^+,\\
&\nu\left[p_{1/2}^{-2}\right]_{0^+}, f_{5/2}^{-1}, i_{13/2}^{-1}; && J_{\max} = 9^-,\\
&\nu p_{1/2}^{-1}, f_{5/2}^{-2}, i_{13/2}^{-1}; && J_{\max} = 11^-,\\
&\nu\left[p_{1/2}^{-2}\right]_{0^+}, i_{13/2}^{-2}; && J_{\max} = 12^+,\\
&\nu p_{1/2}^{-1}, f_{5/2}^{-1}, i_{13/2}^{-2}; && J_{\max} = 15^+,\\
&\nu f_{5/2}^{-2}, i_{13/2}^{-2}; && J_{\max} = 16^+,
\end{aligned}$$

defining its yrast levels up to about 5 MeV.

The large number of (non-equal) alternatives is one factor that will lead to a difference in the more neutron-deficient cases compared to isotopes close to $N = 126$, in that the core excitations that tend to dominate once the valence proton spin is exhausted are less likely to be competitive, since significant angular momentum is available from the neutrons, particularly the $f_{5/2}$ and $i_{13/2}$ neutron holes. Core polarization is also more important as holes are added, leading to significant energy shifts (several hundred keV), and maximum spin couplings are usually unfavored because of the strongly repulsive proton neutron-hole interaction for mutual alignment.

These factors act as a background to the consideration of the selection of states in the energy systematics for the odd-A francium isotopes shown in Fig. 10. Most connections made between the states observed and the appearance of specific configurations in moving away from the closed neutron shell are straightforward.

At low spin, $11/2^-$, $13/2^-$, and $15/2^-$ states related to those in ^{211}Fr are observed in ^{209}Fr, as well as a second $17/2^-$ state at 1225 keV, proposed to be from the $[\nu p_{1/2}^{-2} f_{5/2}^{-2}]_{4^+}$ excitation, maximally coupled to the $9/2^-$ proton ground state. The 539 keV $E2$ branch to this state, which is lower in excitation energy than the $17/2^-$ state from the pure proton excitation, is considerably weaker than the 433 keV $E2$ branch to the upper $17/2^-$ state, despite the higher transition energy, consistent with the difference in configuration between the initial $21/2^-$ state and the lower of the $17/2^-$ states.

The $21/2^-$ and $23/2^-$ states at 1764 and 1929 keV can be associated with the $h_{9/2}^5$ and $h_{9/2}^4 f_{7/2}$ proton configurations, respectively (with the neutron holes coupled to zero), observed at 1686 and 1860 keV in ^{211}Fr [1]. The maximally coupled $25/2^-$ state from the $h_{9/2}^5$ configuration (which does not produce a $23/2^-$ state) is expected about 750 keV above the $21/2^-$ state [1], the $25/2^{(-)}$ state assigned at 2559 keV therefore being a good experimental candidate. The limit on the 165 keV $23/2^- \rightarrow 21/2^- M1$ transition is $>1.06 \times 10^{-3}$ W.u., which is not a significant constraint on the configurations proposed (Table III).

These and other suggested configuration assignments, some of which are discussed further below, are summarized in Table IV. A zero-order estimate of the energies of states expected in ^{209}Fr can be obtained by summing the observed lowest-lying states in ^{204}Pb with well-defined configurations and those of the low-lying valence proton states known from ^{213}Fr. These will be affected by the residual interactions between the neutron holes and valence protons which can be estimated approximately from the known two-particle residual

TABLE IV. Selected configuration assignments in ^{209}Fr arranged as multiplets.

$E_{exp.}$ (keV)	J^π	Main configuration[a]
0	$9/2^-$	$\pi h_{9/2}^5 \otimes \nu(p_{1/2}^{-2} f_{5/2}^{-2})_{0^+}$
1330	$17/2^-$	$\pi h_{9/2}^5 \otimes \nu(p_{1/2}^{-2} f_{5/2}^{-2})_{0^+}$
1764	$21/2^-$	$\pi h_{9/2}^5 \otimes \nu(p_{1/2}^{-2} f_{5/2}^{-2})_{0^+}$
2559	$25/2^-$	$\pi h_{9/2}^5 \otimes \nu(p_{1/2}^{-2} f_{5/2}^{-2})_{0^+}$
623	$11/2^-$	$\pi h_{9/2}^5 \otimes \nu(p_{1/2}^{-2})_{0^+}(f_{5/2}^{-2})_{2^+}$
606	$13/2^-$	$\pi h_{9/2}^5 \otimes \nu(p_{1/2}^{-2})_{0^+}(f_{5/2}^{-2})_{2^+}$
1089	$15/2^-$	$\pi h_{9/2}^5 \otimes \nu(p_{1/2}^{-2})_{0^+}(f_{5/2}^{-2})_{4^+}$
1225	$17/2^-$	$\pi h_{9/2}^5 \otimes \nu(p_{1/2}^{-2})_{0^+}(f_{5/2}^{-2})_{4^+}$
1929	$23/2^-$	$\pi h_{9/2}^4 f_{7/2} \otimes \nu(p_{1/2}^{-2} f_{5/2}^{-2})_{0^+}$
2599	$27/2^-$	$\pi h_{9/2}^4 f_{7/2} \otimes \nu(p_{1/2}^{-2} f_{5/2}^{-2})_{0^+}$
3127	$31/2^-$	$\pi h_{9/2}^4 f_{7/2} \otimes \nu(p_{1/2}^{-2} f_{5/2}^{-2})_{0^+}$
2130	$25/2^+$	$\pi h_{9/2}^5 \otimes \nu(p_{1/2}^{-2})_{0^+}(f_{5/2}^{-1} i_{13/2}^{-1})_{9^-}$
2696	$27/2^+$	$(\pi h_{9/2}^5 \otimes \nu(p_{1/2}^{-2})_{0^+}(f_{5/2}^{-1} i_{13/2}^{-1})_{9^-}$
3416	$33/2^-$	$(\pi h_{9/2}^5 \otimes \nu(j^{-2})_{0^+}(i_{13/2}^{-2})_{12^+})$
2176	$25/2^+$	$\pi h_{9/2}^4 i_{13/2} \otimes \nu(p_{1/2}^{-2} f_{5/2}^{-2})_{0^+}$
2408	$27/2^+$	$\pi h_{9/2}^4 i_{13/2} \otimes \nu(p_{1/2}^{-2} f_{5/2}^{-2})_{0^+}$
2425	$29/2^+$	$\pi h_{9/2}^4 i_{13/2} \otimes \nu(p_{1/2}^{-2} f_{5/2}^{-2})_{0^+}$
3027	$31/2^+$	$\pi h_{9/2}^4 i_{13/2} \otimes \nu(p_{1/2}^{-2} f_{5/2}^{-2})_{0^+}$
3115	$33/2^+$	$\pi h_{9/2}^4 i_{13/2} \otimes \nu(p_{1/2}^{-2} f_{5/2}^{-2})_{0^+}$
3631	$37/2^+$	$\pi h_{9/2}^4 i_{13/2} \otimes \nu(p_{1/2}^{-2} f_{5/2}^{-2})_{0^+}$
3234	$31/2^+$	$(\pi h_{9/2}^4 i_{13/2} \otimes \nu(p_{1/2}^{-2})_{0^+}(f_{5/2}^{-2})_{2^+})$
3409	$33/2^+$	$(\pi h_{9/2}^4 i_{13/2} \otimes \nu(p_{1/2}^{-2})_{0^+}(f_{5/2}^{-2})_{2^+})$
4040	$39/2^+$	$\pi h_{9/2}^3 f_{7/2} i_{13/2} \otimes \nu(p_{1/2}^{-2} f_{5/2}^{-2})_{0^+}$
4324	$41/2^+$	$\pi h_{9/2}^3 f_{7/2} i_{13/2} \otimes \nu(p_{1/2}^{-2} f_{5/2}^{-2})_{0^+}$
4660	$45/2^-$	$\pi h_{9/2}^3 i_{13/2}^2 \otimes \nu(p_{1/2}^{-2} f_{5/2}^{-2})_{0^+}$

[a]Tentative assignments are indicated by parentheses.
[b]Calculated energies as described in the text.

interactions using standard techniques (see, for example, Refs. [15,20]) but with the neutron and proton spin components J_n^π and J_p^π restricted to those of the empirical ^{204}Pb and ^{213}Fr states.

An unusual feature in the experimental spectrum is the observation of two $25/2^+$ states at 2130 and 2176 keV, the lower of which is an isomer. The upper state is suggested to be the expected $\pi h_{9/2}^4 i_{13/2}$ multiplet member (consistent with the preferential decays to this state from the higher-lying states in the main cascade), but there are few other possibilities for obtaining states of this spin and parity at such a low energy, and no equivalent is observed in ^{211}Fr [1]. This leads us to the suggestion of an excitation involving the $i_{13/2}^{-1}$ neutron hole, which is less significant in the heavier isotopes. The $\nu f_{5/2}^{-1} i_{13/2}^{-1}$ excitation could add 9^- to the proton components, but as noted earlier, the maximum spin couplings will not be favored. The proposed configuration for the 2130 keV is this neutron-hole excitation coupled to the proton $9/2^-$ ground state, with $J = J_{max} - 1 = 25/2^+$. The 9^- excitation in ^{204}Pb is at 2186 keV [19], while in the (four valence-proton) isotone ^{208}Rn it has been assigned at 2319 keV [21]. On the basis of the residual interactions (see Ref. [1] for representative calculations) the $J_{max} = 27/2^+$ state from the same multiplet would be expected about 800 keV higher. The $27/2^+$ state at 2696 keV has a preferential decay to the lower $25/2^+$ state and is a candidate for the J_{max} state, given that the residual interactions are likely to be overestimated.

Both $25/2^+$ states have retarded $E1$ decays to the $23/2^-$ state, but that from the 2130 keV isomeric state is an order of magnitude slower than the decay from the upper state, consistent with the larger configuration difference. Only a limit is available for the 45 keV $M1$ transition that connects the two $25/2^+$ states; but again, at $>7 \times 10^{-3}$ W.u., it neither presents a difficulty nor supports the assignment, remembering also that there may be some mixing between the $25/2^+$ states given their proximity.

Note also that there are no direct decays to the 2130 keV state from the $27/2^+$ and $29/2^+$ states at 2408 and 2425 keV. The $27/2^+$ and $29/2^+$ states are attributed to the same source as the upper of the two $25/2^+$ states, namely, the $\pi h_{9/2}^4 i_{13/2}$ configuration. These states are from the lower seniority couplings within the $h_{9/2}^4$ component, with the maximum spin from that coupling in this configuration $(\pi[h_{9/2}^2]_0 h_{9/2}^2 i_{13/2})$ being $29/2^+$. The equivalent $29/2^+$ and $25/2^+$ multiplet members are closer in energy in ^{211}Fr and connected by a strong 113 keV $E2$ transition [0.36(5) W.u.], while in ^{213}Fr, only the $29/2^+$ state is observed, the $25/2^+$ being either higher in energy or bypassed. As discussed in Ref. [1], these states are sensitive to core polarization [22], which has the effect of raising the $29/2^+$ energy and lowering the $25/2^+$ energy with a concomitant contribution to the $E2$ strength because of the introduction of a $2^+ \rightarrow 0^+$ core component. A change to a ^{204}Pb core from the ^{206}Pb core active in ^{211}Fr, will enhance the core polarization (see Ref. [21]), thus accounting for the larger (249 keV) gap observed in ^{209}Fr, and presumably the higher strength of $>0.9(2)$ W.u. for the 249 keV $E2$ transition. The limit on the strength of the 17 keV $M1$ transition connecting the $29/2^+$ and $27/2^+$ states is not a constraint, as noted with other low-energy $M1$ transitions; but at >0.05 W.u., it might be becoming significant. An equivalent $27/2^+$ state has not been observed in the heavier isotopes. It is seen in ^{209}Fr because it falls below the $29/2^+$ state, whereas in the heavier cases it is predicted to lie above the $29/2^+$ state [1].

This leads to the assignments for the main cascade, together with the $29/2^+$ state already discussed, the $33/2^+$, 3115 keV state, and the $37/2^+$, 3631 keV states being the multiplet members from the $\pi h_{9/2}^4 i_{13/2}$ configuration extending up to the maximum spin available.

As has been discussed previously, the yrast states in the closed neutron shell nucleus ^{213}Fr are dominated by proton configurations up to about 5 MeV. The highest spins available at moderate energies are from the $\pi h_{9/2}^3 i_{13/2}^2$ valence proton configuration which can couple to $J_{max}^\pi = 45/2^-$. In both ^{213}Fr and ^{211}Fr, this state preferentially decays via an enhanced $E3$ transition to the $\pi h_{9/2}^3 f_{7/2} i_{13/2}$ valence proton configuration with $J_{max}^\pi - 1 = 39/2^+$. The same configurations are assigned

here to the isomeric state in ^{209}Fr at 4643 keV and to the $39/2^+$ state at 4040 keV. The $41/2^+$ maximum-spin partner of the 4040 keV state is presumably the 4324 keV state. The $E3$ strengths for the $45/2^- \rightarrow 39/2^+$ decays are 34–42 W.u. in ^{213}Fr [1], 33(4) W.u. in ^{211}Fr [1], and 28.8(12) W.u. in ^{209}Fr (present work, Table III). In ^{209}Fr we also observe a very weak branch from the $45/2^-$ isomer to the $41/2^+$ state at 4324 keV, with a low $M2$ strength of ∼0.005 W.u., consistent with the J-forbidden $M2$ implied by the proposed configuration assignments.

Although the information on the states above the $45/2^-$ isomer, most of which involve single-transition feeds, all seem to be either spin 47/2 or spin 49/2, with five likely 47/2 states (at least two with negative parity) and two $49/2^-$ states. Most could be accommodated within the groups of states expected from the higher lying configurations listed earlier, viz., $\pi h_{9/2}^4 i_{13/2} \times \nu(p_{1/2}^{-2})_{0^+}[f_{5/2}^{-1} i_{13/2}^{-1}]_{9^-}$ ($J_{\max} = 55/2^-$), $\pi h_{9/2}^3 f_{7/2} i_{13/2} \times \nu(p_{1/2}^{-2})_{0^+}[f_{5/2}^{-2}]_{4^+}$ ($J_{\max} = 49/2^+$), $\pi h_{9/2}^3 i_{13/2}^2 \times \nu(p_{1/2}^{-2})_{0^+}[f_{5/2}^{-2}]_{4^+}$ ($J_{\max} = 53/2^-$), $\pi h_{9/2}^2 i_{13/2}^3 \times \nu[j^{-4}]_{0^+}$ ($J_{\max} = 49/2^+$), and $\pi h_{9/2}^2 i_{13/2}^3 \times \nu(p_{1/2}^{-2})_{0^+}[f_{5/2}^{-2}]_{4^+}$ ($J_{\max} = 57/2^+$). (Whether the highest spin states from these configurations could be identified in the future will depend on the angular momentum limitation imposed by the competition with fission, although there is scope for further enhancement of the angular momentum input with the present reactions.)

There are a number of non-yrast states for which the spin and parity assignments are less firm, and it is not possible to make reliable configuration assignments. However, the group of non-yrast states with possible positive parity such as those at 3234 and 3409 keV and the states above and below that decay eventually through the $25/2^+$, $27/2^+$, and $29/2^+$ states assigned to the $\pi h_{9/2}^4 i_{13/2}$ configuration probably have the same proton configuration but with an angular momentum contribution from the p- and f-neutron holes, as indicated (tentatively) in Table IV.

Finally, the weakly populated isomeric state at 3415 keV has a tentative $33/2^{(-)}$ assignment and decays only to the 3324 keV state. A possible configuration assignment is the 12^+ four neutron-hole state in ^{204}Pb($p_{1/2}^{-2} i_{13/2}^{-2}$ configuration) coupled to the $9/2^-$ proton ground state. The energy difference between the 9^- and 12^+ states in ^{204}Pb is 1320 keV, which, ignoring residual interactions, would imply (relative to the 2696 keV $27/2^+$ state) a $33/2^-$ state at about 4016 keV, significantly higher than the observed state. The residual interactions are likely to increase the gap. An additional issue is its preferred decay path via a low-energy $E1$ transition, when there are several lower-lying states to which it could, in principle, decay by higher energy, low-multipolarity transitions. The origin of this isomer is therefore an open question.

V. SUMMARY

A comprehensive level scheme has been established for ^{209}Fr including three isomers, the uppermost of which arises from an enhanced $E3$ decay. The assignments disagree with earlier work on this nucleus, a discrepancy attributed from the present measurements, to an isotopic misassignment in the previous work. The main yrast states observed can be associated with either valence proton configurations or proton configurations coupled to relatively low-spin couplings of the neutron holes. This is consistent with the state properties and in good agreement with the expectations from the systematics for the odd-A isotopes. Although more complicated because of the presence of the higher-spin neutron holes, leading to alternative ways of producing states of a given spin, the structures are generally similar to those in the heavier isotopes arising from spherical shell-model configurations.

ACKNOWLEDGMENTS

The authors are grateful to the staff of the ANU Heavy Ion Accelerator Facility for their continuing support. Alan Devlin and Angela Teh are thanked for their assistance with the electron measurements. P.N. acknowledges funding from the Academy of Finland (Grant No. 121110).

[1] A. P. Byrne, G. D. Dracoulis, C. Fahlander, H. Hübel, A. R. Poletti, A. E. Stuchbery, J. Gerl, R. F. Davie, and S. J. Poletti, Nucl. Phys. **A448**, 137 (1986).
[2] A. P. Byrne, R. Müsseler, H. Hübel, M. Murzel, K. Theine, W. Schmitz, K. H. Maier, H. Kluge, H. Grawe, and H. Haas, Phys. Lett. **B217**, 38 (1989).
[3] P. Kuusiniemi, F. P. Heßberger, D. Ackermann, S. Hofmann, and I. Kojouharov, Eur. Phys. J. A **22**, 429 (2004).
[4] D. A. Meyer, C. W. Beausang, J. J. Ressler, H. Ai, H. Amro, M. Babilon, R. F. Casten, C. R. Fitzpatrick, G. Gürdal, A. Heinz, E. A. McCutchan, C. Plettner, J. Qian, N. J. Thomas, V. Werner, E. Williams, N. V. Zamfir, and Jing-ye Zhang, Phys. Rev. C **73**, 024307 (2006).
[5] G. D. Dracoulis, P. M. Davidson, G. J. Lane, A. P. Byrne, T. Kibédi, P. Nieminen, A. N. Wilson, and H. Watanabe, Eur. Phys. J. A (in press).
[6] D. J. Hartley, E. P. Seyfried, W. Reviol, D. G. Sarantites, C. J. Chiara, O. L. Pechenaya, K. Hauschild, A. Lopez-Martens, M. P. Carpenter, R. V. F. Janssens, D. Seweryniak, and S. Zhu, Phys. Rev. C **78**, 054319 (2008).
[7] G. D. Dracoulis, G. J. Lane, A. P. Byrne, P. M. Davidson, T. Kibédi, P. Nieminen, H. Watanabe, and A. N. Wilson, Phys. Lett. **B662**, 19 (2008).
[8] G. D. Dracoulis, G. J. Lane, A. P. Byrne, P. M. Davidson, T. Kibédi, P. Nieminen, H. Watanabe, and A. N. Wilson (in preparation).
[9] T. Kibédi, G. D. Dracoulis, and A. P. Byrne, Nucl. Instrum. Methods Phys. Res. A **294**, 523 (1990).
[10] S. Baba, K. Hata, S. Ichikawa, T. Sekine, Y. Nagame, A. Yokoyama, M. Shoji, T. Saito, N. Takahashi, H. Baba, and I. Fujiwara, Z. Phys. A **331**, 53 (1988).
[11] K.-T. Brinkmann, A. L. Caraley, B. J. Fineman, N. Gan, J. Velkovska, and R. L. McGrath, Phys. Rev. C **50**, 309 (1994).
[12] D. J. Hinde, R. J. Charity, G. S. Foote, J. R. Leigh, J. O. Newton, S. Ogaza, and A. Chatterjee, Nucl. Phys. **A452**, 550 (1986).

[13] G. Stancari, S. Veronesi, L. Corradi, S. N. Atutov, R. Calabrese, A. Dainelli, E. Mariotti, L. Moi, S. Sanguinetti, and L. Tomassetti, Nucl. Instrum. Methods A **557**, 390 (2006).
[14] L. Corradi *et al.*, Phys. Rev. C **71**, 014609 (2005).
[15] A. R. Poletti, A. P. Byrne, G. D. Dracoulis, T. Kibédi, and P. M. Davidson, Nucl. Phys. **A756**, 83 (2005).
[16] E. R. Tardiff *et al.*, Phys. Rev. C **77**, 052501(R) (2008).
[17] T. Kibédi, T. W. Burrows, M. B. Trzhaskovskaya, P. M. Davidson, and C. J. Nestor, Jr., Nucl. Instrum. Methods A **589**, 202 (2008).
[18] X. C. Feng *et al.*, Eur. Phys. J. A **6**, 235 (1999).
[19] C. G. Lindén, I. Bergström, J. Blomqvist, and C. Roulet, Z. Phys. A **284**, 217 (1978).
[20] S. Bayer, A. P. Byrne, G. D. Dracoulis, A. M. Baxter, T. Kibèdi, and F. G. Kondev, Nucl. Phys. **A694**, 3 (2001).
[21] W. J. Triggs, A. R. Poletti, G. D. Dracoulis, C. Fahlander, and A. P. Byrne, Nucl. Phys. **A395**, 274 (1983).
[22] J. Blomqvist, I. Bergström, C. J. Herrlander, C. G. Lindèn, and K. Wikström, Phys. Rev. Lett. **38**, 534 (1977).